Check for updates

Endochondral bone in an Early Devonian 'placoderm' from Mongolia

Martin D. Brazeau [1,2 ✉], Sam Giles [2,3,4], Richard P. Dearden [1,5], Anna Jerve[1,6], Ya. Ariunchimeg[7], E. Zorig[8], Robert Sansom [9], Thomas Guillerme [10] and Marco Castiello [1]

Endochondral bone is the main internal skeletal tissue of nearly all osteichthyans—the group comprising more than 60,000 living species of bony fishes and tetrapods. Chondrichthyans (sharks and their kin) are the living sister group of osteichthyans and have primarily cartilaginous endoskeletons, long considered the ancestral condition for all jawed vertebrates (gnathostomes). The absence of bone in modern jawless fishes and the absence of endochondral ossification in early fossil gnathostomes appear to lend support to this conclusion. Here we report the discovery of extensive endochondral bone in *Minjinia turgenensis*, a new genus and species of 'placoderm'-like fish from the Early Devonian (Pragian) of western Mongolia described using X-ray computed microtomography. The fossil consists of a partial skull roof and braincase with anatomical details providing strong evidence of placement in the gnathostome stem group. However, its endochondral space is filled with an extensive network of fine trabeculae resembling the endochondral bone of osteichthyans. Phylogenetic analyses place this new taxon as a proximate sister group of the gnathostome crown. These results provide direct support for theories of generalized bone loss in chondrichthyans. Furthermore, they revive theories of a phylogenetically deeper origin of endochondral bone and its absence in chondrichthyans as a secondary condition.

The vertebrate skeleton comprises two main systems: the exoskeleton (external achondral dermal bones) and the endoskeleton (internal chondral bones and cartilages, as well as some intramembranous bones)[1]. An ossified exoskeleton evolved at least 450 million years ago in jawless stem gnathostomes[2,3], but the endoskeleton in these taxa is not endochondrally ossified. Endochondral bone, in which the cartilaginous endoskeletal precursor is invaded by and eventually replaced by bone, is widely considered an osteichthyan apomorphy[3–7], and such a reliable identifying character that it gives the group its name. Extant chondrichthyans lack dermal bone and possess a mainly cartilaginous endoskeleton enveloped by a structurally diverse range of tessellate calcified cartilage[8]. Outgroups of the gnathostome crown also lack endochondral ossification. Galeaspids surround their cartilaginous skeleton in globular calcified cartilage[9], while osteostracan and 'placoderm' endoskeletons were sheathed in perichondral bone[3]. Consequently, the last common ancestor of jawed vertebrates was long thought to have been perichondrally ossified, but lacking endochondral ossification[3].

In this paper, we describe a new genus and species of 'placoderm' from the Early Devonian of western Mongolia. Although Mongolia is known for some of the geologically oldest putative gnathostome fossils (isolated chondrichthyan-like scales[10–13]), it remains a poorly sampled region of the world with respect to early vertebrates. 'Placoderms' were until now known from only a single fragmentary occurrence[14] in the early Middle Devonian (Eifelian). Our new data highlight the importance of Mongolia as a key region for studies of early gnathostome evolution. We describe a partial braincase and skull roof representing the first substantial body fossil of an early gnathostome from Mongolia and displaying an unexpected occurrence of endochondral bone, which we analysed using X-ray computed microtomography. We conducted phylogenetic analyses to reconstruct the evolutionary relationships of this new taxon. To explore the evolutionary history of endochondral bone in light of this new discovery, we used parsimony and maximum-likelihood ancestral state reconstruction. Finally, we discuss these results in the context of earlier statements about endochondral bone in non-osteichthyans, new developments in understanding the complexity and diversity of chondrichthyan endoskeletal tissues, and current uncertainties about early gnathostome phylogenetic relationships.

Systematic palaeontology

Gnathostomata Gegenbaur, 1874 (ref. [15])

Minjinia turgenensis gen. et sp. nov.

Etymology. The generic name honours the memory of C. Minjin for his extensive contributions to the Palaeozoic stratigraphy of Mongolia, his enthusiastic support of this work, and introducing us to the Yamaat River locality. The specific name recognizes the provenance of the fossil from the Turgen region Uvs aimag of western Mongolia.

Holotype. Institute of Paleontology, Mongolian Academy of Sciences MPC-FH100/9.1, a partial braincase and skull roof.

Locality. Turgen Strictly Protected Area, Uvs province, western Mongolia; near the top of the stratigraphic sequence that occurs near the confluence of the Tsagaan-Salaa and Yamaat rivers.

[1]Department of Life Sciences, Imperial College London, Ascot, UK. [2]Department of Earth Sciences, Natural History Museum, London, UK. [3]School of Geography, Earth and Environmental Sciences, University of Birmingham, Birmingham, UK. [4]Department of Earth Sciences, University of Oxford, Oxford, UK. [5]CR2P Centre de Recherche en Paléontologie – Paris, Muséum National d'Histoire Naturelle, Sorbonne Universités, CNRS, Paris, France. [6]Subdepartment of Evolution and Development, Department of Organismal Biology, Uppsala University, Uppsala, Sweden. [7]Natural History Museum, Ulaanbaatar, Mongolia. [8]Institute of Paleontology, Mongolian Academy of Science, Ulaanbaatar, Mongolia. [9]School of Earth and Environmental Sciences, University of Manchester, Manchester, UK. [10]Department of Animal and Plant Sciences, The University of Sheffield, Sheffield, UK. ✉e-mail: m.brazeau@imperial.ac.uk
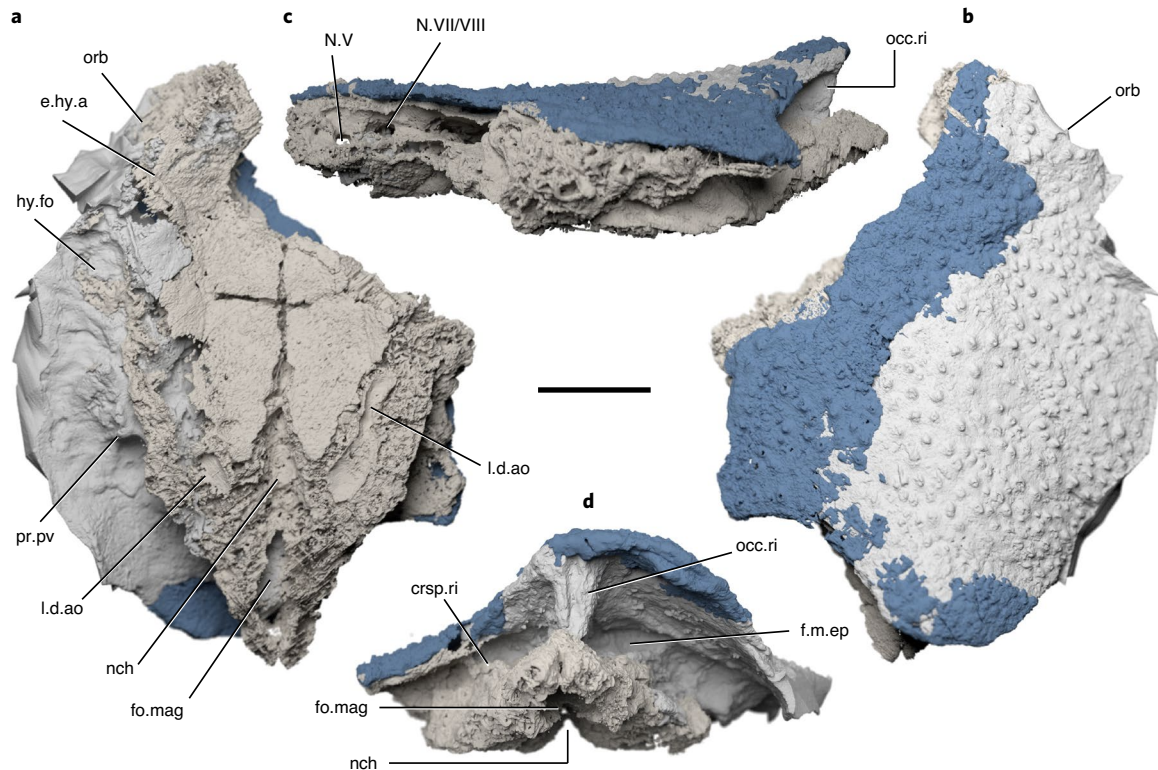
Fig. 1 | MPC-FH100/9.1, a 'placoderm' skull roof and braincase from the Early Devonian of Mongolia. a, Ventral view. **b**, Dorsal view. **c**, Left lateral view. **d**, Posterior view. Taupe: endoskeleton; grey: mould; blue: exoskeleton. crsp.ri, craniospinal ridge; e.hy.a, sulcus for the efferent hyoid artery; f.m.ep, epaxial muscle fossa; fo.mag, foramen magnum; hy.fo, hyoidean fossa; l.d.ao, sulcus for the lateral dorsal aorta; N.V, trigeminal nerve canal; N.VII, facial nerve canal; N.VIII, acoustic nerve canal; nch, notochordal canal; occ.ri, occipital ridge; orb, orbit; pr.pv, paravagal process. Scale bar, 10 mm.

Horizon. Upper part of Tsagaan-Salaa Gol Formation, Pragian (Early Devonian)[16,17].

Diagnosis. 'Placoderm'-grade stem gnathostome with endochondral bone, deep epaxial muscle cavities flanking a slender occipital ridge, and the following possible autapomorphies: dermal bones covered in sparsely placed tubercles; penultimate spino-occipital nerve canal substantially larger in diameter than others.

Description. MPC-FH100/9.1 consists of a partial braincase and skull roof (Fig. 1). The skull roof is ornamented with sparsely distributed finely ridged tubercles resembling those of the Siberian 'placoderm' *Dolganosteus*[18]; the tubercles become more broadly separated towards the midline of the skull. They are distinct from those of *Dolganosteus* in that towards the midline of the skull roof, the tubercles are larger and more pointed. The specimen shows signs of extensive post-mortem transport, with angles of the braincase worn off and much of the skull roof and some of the braincase preserved as a mould. Individual skull roof ossifications cannot be identified, although this may be due to the dominantly mouldic preservation. There appears to have been a prominent nuchal plate eminence comparable to that of certain acanthothoracids such as *Romundina*[19] and *Arabosteus*[20].

Endoskeletal tissue. The braincase of MPC-FH100/9.1 is well ossified, comprising an external bony sheath filled with an extensive matrix of spongy tissue (Fig. 2a,b, Extended Data Fig. 1 and Supplementary Video 1). The trabecles forming this tissue are irregular and branching, less than 1 mm thick and often curved, and resemble most closely the endochondral tissue of osteichthyans (Fig. 2c,d and Supplementary Video 2). As such, we interpret this as

endochondral bone. Notably, this is found in all preserved regions of the braincase, in contrast to the isolated trabeculae previously identified as endochondral bone in *Boreaspis*[21] and *Bothriolepis*[22]. The margins of the braincase, the endocranial walls and the boundaries of nerve and blood canals are formed from a thicker tissue that we interpret as perichondral bone. This suggests that the endoskeleton of *Minjinia* comprises osteichthyan-like endochondral bone, with an ossified perichondrium. To address the possible alternative explanation that it is an aberrant instance of calcified cartilage, we compared the structure of this tissue with rarely preserved mineralized cartilage in the stem chondrichthyan *Diplacanthus crassisimus* (National Museums of Scotland specimen NMS 1891.92.334; Fig. 2e,f) observed using synchrotron tomography. The cancellae within the endochondral tissue of *Minjinia* are irregular, with a diameter of approximately 1–2 mm. This tissue is distinctly unlike the calcified cartilage of *Diplacanthus* in appearance, which consists of a densely packed matrix of irregularly stacked chondrons between 20 and 60 μm in diameter.

Neurocranium. The braincase is preserved from the level of the right posterior orbital wall to the posterior end of the occipital ridge. Occipital glenoid condyles are not preserved, but much of the rest of the broad, flat parachordal region is present, separated by a midline groove that accommodated a relatively narrow notochordal tunnel. An asymmetric transverse fissure spans the basicranial surface at about mid-length of the preserved portion. It appears to demarcate the anterior margin of the parachordal plates and may correspond to the ventral cranial fissure of crown-group gnathostomes. However, unlike in crown gnathostomes, it is traversed by a substantial anterior extension of the cranial notochord. The courses of the lateral dorsal aortae are marked by a pair of sulci on the lateral
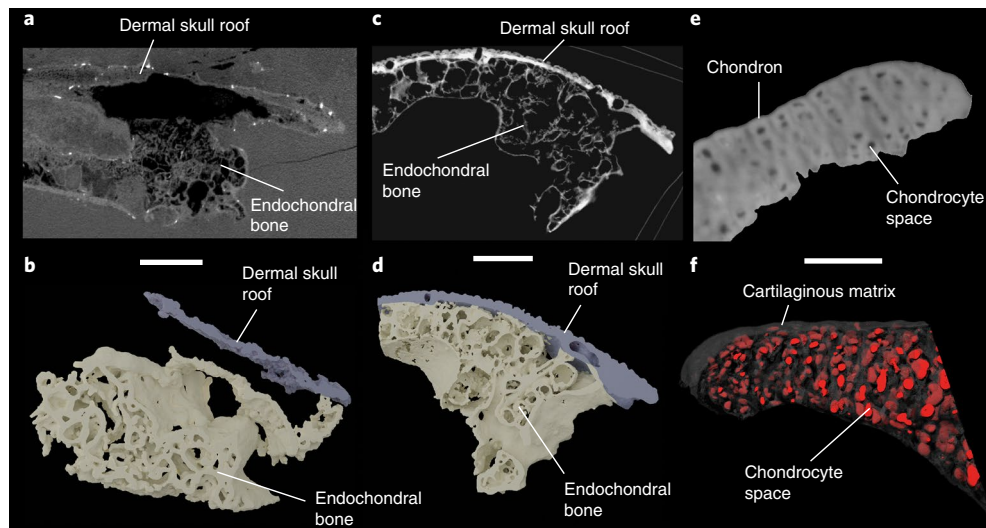
Fig. 2 | Endoskeletal mineralization in fossil gnathostomes. a, A transverse tomographic slice through MPC-FH100/9.1. **b**, Three-dimensional rendering of trabecular bone structure of MPC-FH100/9.1. **c**, A transverse tomographic section through the braincase of the osteichthyan *Ligulalepis*. **d**, Three-dimensional rendering of the trabecular bone in *Ligulalepis* (**c** and **d** use data from ref. [56]). **e**, A synchrotron tomography image of the calcified cartilage of the certatohyal of the stem-group chondrichthyan *Diplacanthus crassisimus* specimen NMS 1891.92.334. **f**, Semi-transparent three-dimensional structure of calcified cartilage of NMS 1891.92.334. Scale bars, 10 mm (**a**,**b**); 1 mm (**c**,**d**); 150 µm (**e**,**f**).

margins of the parachordal plates, although only a short part of the canal is preserved on the right side of the specimen. A narrow, shallow sulcus for the efferent hyoid artery is present on the preserved right side of the specimen, immediately behind the level of the orbit (Fig. 1a).

The lateral surface of the braincase is preserved on the right side as a mouldic impression in the matrix (Fig. 1). A sharply demarcated hyoid fossa is present on the lateral wall of the otic region (Fig. 1). Posterior to this, a stout but pronounced vagal process with a pair of rounded eminences probably corresponds to the branchial arch articulations. There is no evidence for a pair of anterior and posterior divisions to the vagal process, which are typically seen in other 'placoderms'. A well-developed 'placoderm'-like craniospinal process is absent; its homologous position is instead covered in perichondral bone and marked by a low ridge (Fig. 1).

In posterior view, a tall, narrow median occipital ridge is evident and resembles the morphology of *Romundina*[23] and *Arabosteus*[20]. As in these taxa, the median otic ridge is flanked by two large occipital fossae for the epaxial musculature. The notochordal tunnel is approximately the same size as or smaller than the foramen magnum, as in 'placoderms' and in contrast with crown-group gnathostomes. A metotic fissure is absent.

Endocast. A partial cranial endocast is preserved, consisting of the hindbrain cavity, partial midbrain cavity, labyrinth cavities and posteromedial corner of the orbital region. The two primary trunk canals of the trigeminal nerve ($N.V_1$ and $N.V_{2,3}$) are preserved (Fig. 3). The acoustic (N.VIII) and facial (N.VII) nerve canals share a common trunk canal behind the trigeminal nerves, as in many other 'placoderms'[23–26]. The facial nerve canal branches into palatal and hyomandibular branches between the saccular chamber and the rear orbit wall (Fig. 3 and Extended Data Fig. 2), indicating that this division was internal (deep) to the otic process. The supraophthalmic branch opens into the rear wall of the orbit and part of its supraorbital course is preserved (Fig. 3 and Extended Data Fig. 2). A slender branch extends below the labyrinth and divides into palatine and hyomandibular branches (Fig. 3 and Extended Data Fig. 2). As in other 'placoderm'-grade taxa, the vagus nerve (N.X) trunk canal is very large in diameter and exits from immediately behind the

labyrinth cavity (Fig. 3). The spino-occipital region resembles that of other 'placoderms' in being extended. At least four spino-occipital nerve canals are present in a linear series, and the penultimate canal is largest in diameter (Fig. 3). Intercalating these is a network of occipital artery canals branching from the dorsal aortae (Fig. 3).

The skeletal labyrinth is not complete on either side of the specimen, but can mostly be reconstructed according to the assumption of bilateral symmetry. The most notable feature is that the labyrinth and endolymphatic cavity are joined to the main endocavity chamber (Fig. 3). This is a striking contrast to other 'placoderms' and closely resembles crown-group gnathostomes[27]. The endolymphatic canals are elongate and tubular, extending posterolaterally to reach the skull roof, although external openings cannot be clearly identified. The anterior semicircular canal follows the saccular cavity closely as in petalichthyids[28] (Fig. 3). However, the horizontal and posterior canals appear to extend well away from the saccular chamber (Fig. 3). The dorsal junctions of the anterior and posterior canals are joined in a crus commune, as in *Romundina*[23] and *Jagorina*[24]. A sinus superior is absent.

Phylogenetic analyses

We conducted phylogenetic analyses under four different protocols: equal-weights parsimony, implied-weights parsimony, an unpartitioned Bayesian analysis and a Bayesian analysis with characters partitioned by fit determined under implied-weights parsimony[29] (see Extended Data Figs. 3–6). All phylogenetic analyses consistently place *Minjinia* as a stem-group gnathostome, proximate to the gnathostome crown (Fig. 4 and Extended Data Figs. 3 and 4). *Minjinia* is recovered in a position crownward of arthrodires but outside a grade consisting of *Entelognathus*, *Ramirosuarezia* and *Janusiscus*. Under implied-weights parsimony, these three taxa move onto the osteichthyan stem and *Minjinia* is placed as the immediate sister taxon of the gnathostome crown. Under equal weights parsimony, the crownward position of *Minjinia* is unambiguously supported by the skeletal labyrinth and endolymphatic duct being confluent with the main cranial cavity[27] (Supplementary Information). In common with arthrodires and the gnathostome crown[30], *Minjinia* possesses a division of the facial nerve (Fig. 3 and Extended Data Fig. 2) deep to the transverse otic process. However, *Minjinia* is excluded from
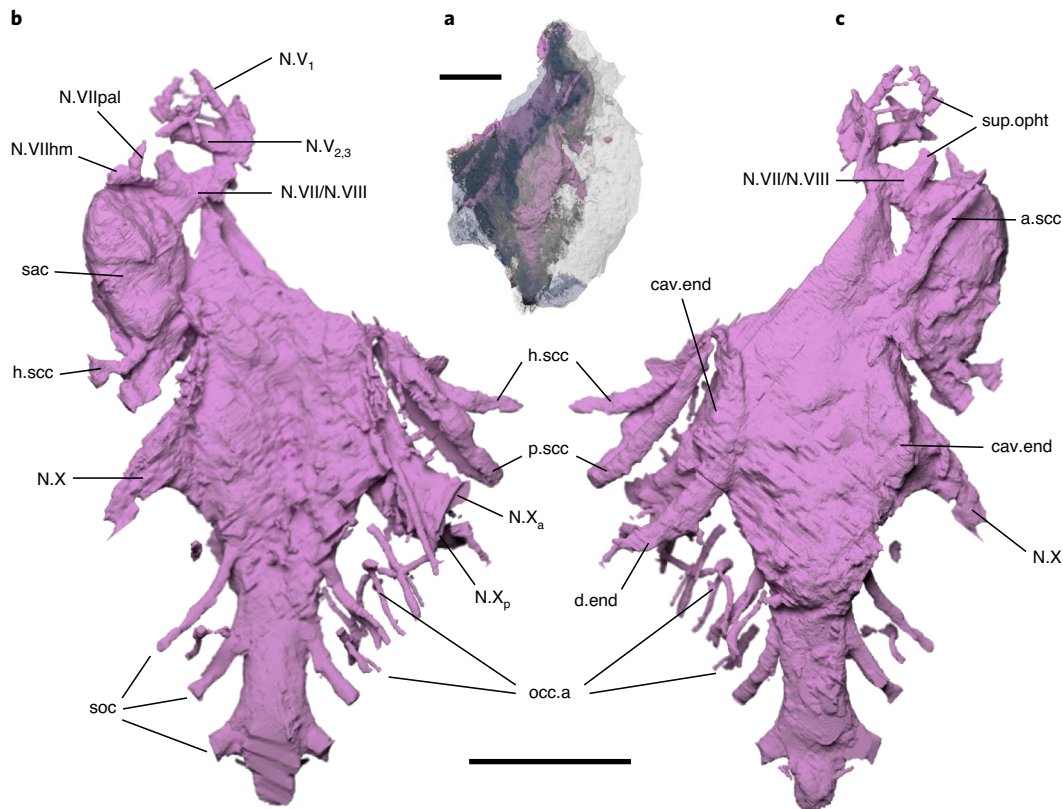
Fig. 3 | Braincase endocavity of MPC-FH100/9.1, *Minjinia turgenensis*. a, Semi-transparent rendering of the skull roof and braincase (grey and blue) showing the extent of the endocavity (pink). **b**, Ventral view. **c**, Dorsal view. a.scc, anterior semicircular canal; cav.end, endolymphatic cavity; d.end, endolymphatic duct; h.scc, horizontal semicircular canal; N.V, trigeminal nerve canal; N.VIIhm, hyomandibular branch of facial nerve canal; N.VII, facial nerve canal; N.VIIpal, palatine branch of facial nerve canal; N.VIII, acoustic nerve canal; N.X, vagus nerve canal, N.X$_a$, anterior branch of vagus nerve canal; N.X$_p$, posterior branch of vagus nerve canal; occ.a, occipital artery canals; p.scc, posterior semicircular canal; sac, sacculus; soc, spino-occipital nerve canals; sup.opht, canal for supra-ophthalmic nerve. Scale bars, 10 mm (upper scale bar associates with **a**; lower scale bar associates with **b,c**).

the gnathostome crown group owing to the absences of a metotic fissure and a posterior dorsal fontanelle, and the presence of broad, flat parachordal plates expanded behind the saccular cavity (Fig. 3 and Supplementary Information).

We undertook ancestral state reconstructions to assess the evolutionary history of endochondral bone (Fig. 4, Extended Data Figs. 5 and 6 and Supplementary Information). Interestingly, parsimony analysis fails to recover secondary homology of this trait between *Minjinia* and osteichthyans. The crownward placement of *Minjinia* is, in fact, based on independent evidence relating to anatomical features of the braincase and endocast. However, the resolution of endochondral bone origin or loss becomes ambiguous if missing data in either *Entelognathus* or *Ramirosuarezia* are resolved as having endochondral bone. The reconstruction becomes similarly ambiguous if *Janusiscus* is moved a single branch (requiring only two additional steps) onto the chondrichthyan stem. The strict precision of parsimony reconstructions makes it insensitive to this underlying uncertainty. To explore this, we used likelihood reconstructions and compared the ancestral state reconstructions under equal rates (ER) and all rates different (ARD) variants of the Mkv model on branch-length-rescaled parsimony trees and Bayesian trees. Both models show substantial non-zero marginal likelihoods if endochondral bone is assumed present in the common node of *Minjinia* and Osteichthyes, with ARD strongly favouring its presence (0.33 for ER; 0.81 for ARD; Fig. 3, Table 1, Extended Data Figs. 5 and 6 and Supplementary Table 1). Under the ARD model, there is nearly equivocal support for presence or absence of endochondral bone at the gnathostome crown node (Table 1). The ARD

model shows the best fit for endochondral bone (likelihood ratios 4.75 for parsimony ($P = 0.029$) and 5.26 for Bayesian ($P = 0.022$); Table 1 and Supplementary Table 1), favouring repeated losses of this tissue over multiple gains (see Discussion).

Discussion

Minjinia turgenensis presents an unexpected discovery of extensive endochondral bone in a 'placoderm'-grade fish, with repercussions for the phylogenetic origin of this tissue and the problem of early gnathostome relationships more generally. The prevailing hypothesis has been that endochondral bone is an osteichthyan apomorphy[3,7,30]. However, recent discoveries have cast doubt on this assertion. The recognition that dermal bone is secondarily lost in chondrichthyans[31,32] (Fig. 4) is consonant with prior knowledge of the loss of perichondral bone in this same lineage[33]. Taken together, these findings have revived uncertainty about the true phylogenetic timing of the origin of endochondral ossification[34]. *Minjinia* provides direct corroboration for a more ancient origin.

Minjinia does not represent the first report of endochondral bone outside Osteichthyes. However, it is by far the most extensive and unequivocal example and raises explicit questions in light of the proximity of *Minjinia* to the gnathostome crown (Fig. 4 and Extended Data Figs. 3 and 4). Isolated examples of trabecular endoskeletal bone have historically been reported in boreaspid osteostracans[21,35], a rhenanid[36], arthrodires[37], a ptyctodont[38] and a petalichthyid[39,40]. However, these reports are nearly all unillustrated statements; they have all been considered tenuous[3] or dismissed as misidentifications[5]. In line with these assessments, we found

no evidence of endochondral bone in material of *Buchanosteus* held in the Natural History Museum, London, or indeed in any other 'placoderms' we have examined. The *Epipetalichthys* holotype (Museum für Naturkunde, Berlin specimen MB.f.132.1–3) shows an apparently spongiose infilling in the anterior region of the braincase, but the identity of this structure, or even whether it is biological, cannot be determined. The *Epipetalichthys* tissue figured by Stensiö[39] was very superficial, and possibly represents the retreat of perichondral bone deposited during cartilage growth[40]. Most recently, trabeculae in supposed endoskeletal pelvic bones of *Bothriolepis* have been termed endochondral bone[22], although the small scale of these is in line with 'superficial' perichondral trabeculae seen elsewhere[39]. The reported examples in boreaspid osteostracans have also been dismissed by later authors[3,5]. Although they warrant further study, their tissue structures are unlikely to be homologous to those of osteichthyans owing to their phylogenetic remoteness and nested position in the Osteostraci[41].

Among chondrichthyans, endochondral bone has been mentioned in 'acanthodians'[3,42], and superficial bone-like tissues have been reported in the skeletons of extant chondrichthyans. We are unable to substantiate statements about 'acanthodians': no authors have cited primary sources or specimens. One possible source is Watson's[43] description of 'massive ossification' of the endoskeleton of *Diplacanthus*. However, our synchrotron data of this same specimen (Fig. 2) show that this tissue is undoubtably calcified cartilage. Some authors have speculated that the superficial mineralized tissue in the jaws of acanthodians or chondrichthyans may have developed in an endochondral position[40]. Histological studies show that endoskeletal mineralization in the jaws of 'acanthodians' is globular calcification and occasionally 'sub-tessellate'[8,44]. Recent comparative studies of histology and development in extant chondrichthyans have shown the presence of an extensive canalicular network in the tesserae[45] and a trabecular tesseral network in some vertebral elements[46], both resembling bone. Whether these represent homologues of osteichthyan examples remains open to debate; future works could employ synchrotron microtomography of cartilages in stem-group chondrichthyans to address these questions.

Does endochondral bone have a deep origin within the gnathostome stem group? This would imply repeated losses of this tissue. We do find statistical support for this hypothesis (Fig. 4, Table 1, Extended Data Figs. 5 and 6 and Supplementary Table 1), and the model is well justified on prior phylogenetic and biological grounds. Endochondral bone has long been known to be inconsistently developed across 'primitive' bony fishes: incomplete, polymorphic or entirely absent ossification of the endoskeleton is known in both Palaeozoic actinopterygians[42,47,48] and sarcopterygians[49], as well as more recent taxa[50]. The frequent absence of endochondral bone in osteichthyans is considered secondary, and other controlling factors such as body size, maturity, mechanical stress and buoyancy can determine its degree of development[1]. Our findings are also in agreement with studies establishing a genetic basis for secondary loss of all bone types within chondrichthyans[51–53], with the failure to produce endochondral bone probably representing arrested development of chondrocytes as opposed to a primary lack of ability[54].

Fig. 4 | Strict consensus tree from equal weights parsimony analysis of early gnathostomes showing distribution of endochondral bone and exoskeletal armour. The squares at nodes indicate parsimony reconstruction for endochondral bone. The pie charts at nodes show likelihood reconstructions for the same character under the ARD model (see Extended Data Figs. 5 and 6 for competing reconstructions). The grey boxes indicate uncertainty. Loss of endochondral bone maps closely with generalized loss of bone in chondrichthyans where exoskeletal armour and perichondral bone are also absent.
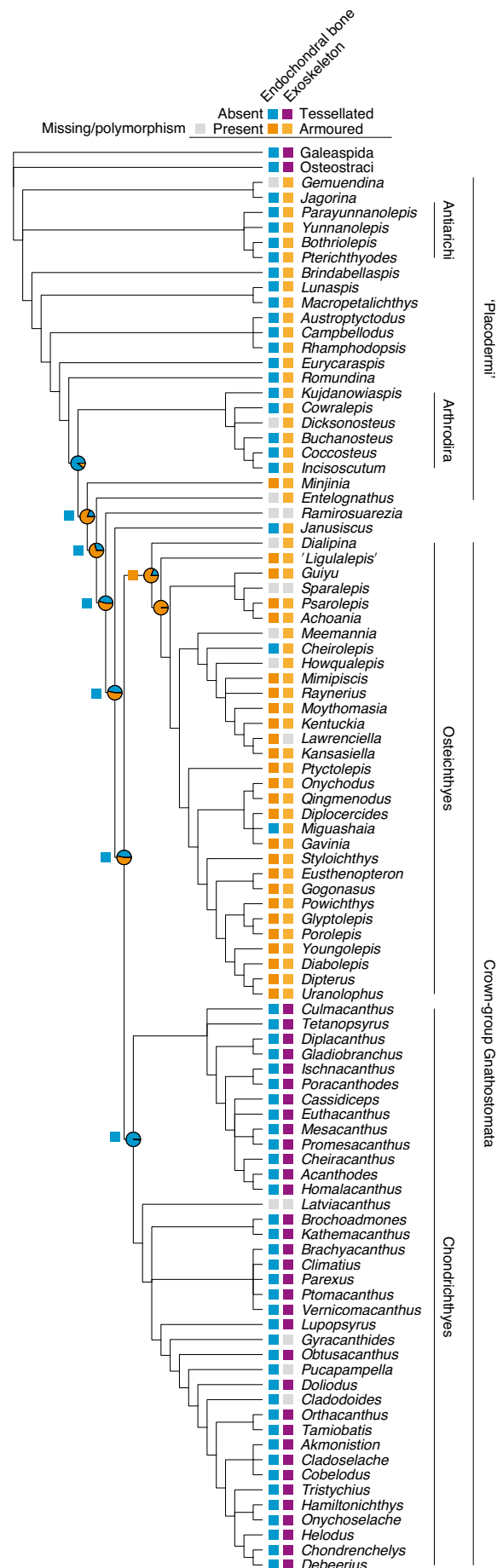
Table 1 | Results of ancestral state estimations for tree distributions (*n* = 100)

Trees	Model	log.like	like.ratio	AIC	Node	Absent	Present
Parsimony	ER	−28.91	4.74	59.82	*Minjinia*:Gnathostomes	0.67	0.33
(equal weights)	ARD	−26.54		57.09		0.19	0.81
	ER				Crown Gnathostomes	0.91	0.09
	ARD					0.46	0.54
Bayesian	ER	−29.66	5.26	61.32	*Minjinia*:Gnathostomes	0.73	0.27
(unpartitioned)	ARD	−27.03		58.06		0.17	0.83
	ER				Crown Gnathostomes	0.79	0.21
	ARD					0.22	0.78

The columns AIC and log.like represent the median AIC and log.like across the 100 parsimony and Bayesian trees (for both models). The like.ratio column is the likelihood ratio for the models compared on these trees. The columns Absent and Present represent the median scaled likelihood for the endochondral bone state.

Another confounding factor in this question is the problem of 'placoderm' relationships. Although currently resolved in most analyses as a deeply pectinate grade along the gnathostome stem (Fig. 4), the backbone of this arrangement has poor statistical support, even in the present analysis (Extended Data Fig. 3). There is a lack of consistency in the arrangement of plesia, and Bayesian tip-dating methods have even recovered a monophyletic Placodermi[55]. *Minjinia* itself highlights this uncertainty, given its highly unexpected character combinations. Notwithstanding its endochondral bone and crown-gnathostome-like inner ear structure, it resembles 'acanthothoracids'—the 'placoderms' widely considered among the most removed from the gnathostome crown (that is, most 'primitive'): it possesses deep epaxial fossae either side of a prominent occipital ridge and a nuchal eminence otherwise seen only in 'acanthothoracids' such as *Romundina*[19] and *Arabosteus*[20]. This apparent character conflict could perhaps be more easily reconciled with a more coherent (although not necessarily monophyletic) 'placoderm' assemblage. Indeed, the highly pectinate structure of the 'placoderm' grade seems symptomatic of an overemphasis on characters and taxa resembling the crown group, thereby undersampling characters that could stabilize a clear picture of 'placoderm' interrelationships.

Minjinia turgenensis reveals new data on 'placoderm' endoskeleton and tissue diversity recorded from Mongolia—an otherwise extremely poorly known biogeographic realm for early gnathostomes. The phylogenetic placement of this 'acanthothoracid'-like taxon crownward of all non-maxillate 'placoderms', in conjunction with possession of extensive endochondral bone, highlights the importance of material from historically undersampled geographic areas. The presence of endochondral bone renews the hypothesis that this tissue is evolutionarily ancient and was lost secondarily in chondrichthyans[6,34]. This view is overall consistent with evidence of generalized bone loss in chondrichthyans, potentially as a result of the suppression of bone-generating molecular genetic pathways[53,54]. Continued work in Mongolia and re-evaluation of phylogenetic datasets will be necessary to address this, with the results likely to lead to substantial re-evaluation of gnathostome phylogeny.

Methods

X-ray computed microtomography. We scanned MPC-FH100/9.1 using the Nikon XT 225s at the Museum of Paleontology, University of Michigan with the following parameters: 200 kV, 140 μA, over 3,123 projections and a voxel size of 32.92 μm. We conducted segmentation using Mimics 19.0 (http://biomedical. materialise.com/mimics; Materialise, Leuven, Belgium) and we imaged models for publication using Blender (https://www.blender.org).

Synchrotron light propagation phase-contrast tomography. We imaged *Diplacanthus crassisimus* specimen NMS 1891.92.334 on Beamline 19 of the European Synchrotron Radiation Facility, using propagation phase-contrast

synchrotron microtomography. We performed a spot scan with an energy of 116 keV, achieving a voxel size of 0.55 μm. We processed the resulting tomograms using VG StudioMax 2.2 (Volume Graphics, Germany), and prepared images in Blender.

Phylogenetic analysis. We conducted a parsimony analysis using TNT 1.5[57] and Bayesian analysis using MrBayes version 3.2.7[58]. The dataset consisted of 95 taxa and 284 discrete characters based on a pre-existing dataset[56]. We employed Osteostraci and Galeaspida as composite outgroups. We conducted parsimony analysis using both equal-weights and implied-weights methods. Global settings were 1,000 search replicates and a hold of up to 1 million trees. Equal-weights parsimony analyses were conducted using the ratchet with default settings. Implied-weights parsimony used a concavity parameter of 3 and the search was without the ratchet. Command lists are included in Supplementary Data 1. We conducted Bayesian analysis using both a partitioned and an unpartitioned dataset. We used the Mkv model[59] and gamma rate distribution. We ran the analyses for 5 million generations with a relative burn-in fraction of 0.25. Runs were checked for convergence using Tracer[60]. We partitioned the dataset using a newly proposed method[29] that partitions the data according to homoplasy levels. Using the results of implied-weights parsimony conducted in TNT, we created a text table of character fit values. We wrote an R[61] script to generate a list of partition commands for MrBayes. Scripts and data files for Bayesian analysis are included in Supplementary Data 1.

We assessed parsimony ancestral states visually using Mesquite[62]. Likelihood and Bayesian ancestral states were estimated in R using the castor package[63] version 1.5.7. Before calculating likelihood ancestral states on parsimony trees, we scaled branch lengths using PAUP*[64] and calculated the likelihood scores for all of the trees under the Mkv model with the gamma rate parameter. The trees were then exported with branch lengths. To account for overall uncertainty in tree estimates, we estimated ancestral states on 100 trees randomly selected from the fundamental set of most parsimonious trees and two times 50 trees selected from the 75% last trees of each posterior tree distribution from the Bayesian analysis. We then ran an ancestral state estimation Mk model (using the castor R package) using both the ER and ARD models. This resulted in 400 ancestral state estimations. For each estimation, we extracted the overlap log likelihood, the Akaike information criterion (AIC; counting one parameter for the ER model and two for the ARD model) and the scaled log likelihood (probability) for the presence and absence of the endochondral bone character (character 4) for the last common node of *Minjinia* and crown-group gnathostomes and the gnathostome crown-group node itself. We present the median value of these distributions of the estimations' overall log likelihoods, AICs and presence or absence of endochondral bone in Table 1. Scripts for ancestral states analyses are included in Supplementary Data 2.

Reporting Summary. Further information on research design is available in the Nature Research Reporting Summary linked to this article.

Data availability
The holotype specimen of *M. turgenensis* will be permanently deposited in the collections of the Institute of Paleontology, Mongolian Academy of Sciences. Original tomograms are available at https://doi.org/10.6084/m9.figshare.12301229 and rendered models are available at https://doi.org/10.6084/m9.figshare.12301223. The phylogenetic character list and dataset are available as Supplementary Information and Supplementary Data 1. The LifeScience Identifier for *M. turgenensis* is urn:lsid:zoobank.org:act:82A1CEEC-B990-47FF-927A-D2F0B59AEA87

References
1. Hall, B. K. *Bones and Cartilage* (Academic, 2005).
2. Janvier, P. *Early Vertebrates* (Oxford Univ. Press, 1996).
3. Donoghue, P. C. J., Sansom, I. & Downs, J. P. Early evolution of vertebrate skeletal tissues and cellular interactions, and the canalization of skeletal development. *J. Exp. Zool.* **306B**, 278–294 (2006).
4. Rosen, D. E., Forey, P. L., Gardiner, B. G. & Patterson, C. Lungfishes, tetrapods, paleontology, and plesiomorphy. *Bull. Am. Mus. Nat. Hist.* **167**, 159–276 (1981).
5. Gardiner, B. G. The relationships of the palaeoniscid fishes, a review based on new specimens of *Mimia* and *Moythomasia* from Upper Devonian of Western Australia. *Bull. Br. Mus. Nat. Hist. Geol.* **37**, 173–428 (1984).
6. Maisey, J. G. Heads and tails: a chordate phylogeny. *Cladistics* **2**, 201–256 (1986).
7. Friedman, M. & Brazeau, M. A reappraisal of the origin and basal radiation of the Osteichthyes. *J. Vertebr. Paleontol.* **30**, 36–56 (2010).
8. Maisey, J. G., Denton, J. S. S., Burrow, C. & Pradel, A. Architectural and ultrastructural features of tessellated calcified cartilage in modern and extinct chondrichthyan fishes. *J. Fish Biol.* https://doi.org/10.1111/jfb.14376 (2020).
9. Wang, N.-Z., Donoghue, P. C. J., Smith, M. M. & Sansom, I. Histology of the galeaspid dermoskeleton and endoskeleton, and the origin and early evolution of the vertebrate cranial endoskeleton. *J. Vertebr. Paleontol.* **25**, 745–756 (2005).
10. Karatajūtė-Talimaa, V. & Novitskaya, L. *Sodolepis*—a new representative of Mongolepidida (Chondrichthyes?) from the lower Silurian of Mongolia. *Paleontol. Zh.* **5**, 96–103 (1997).
11. Karatajūtė-Talimaa, V. & Novitskaya, L. *Teslepis*—a new representative of mongolepid elasmobranchs from the Lower Silurian of Mongolia. *Paleontol. Zh.* **4**, 36–43 (1992).
12. Karatajūtė-Talimaa, V., Novitskaya, L. & Rozman, K. S. *Mongolepis*—a new lower Silurian genus of elasmobranchs from Mongolia. *Paleontol. Zh.* **1**, 76–86 (1990).
13. Andreev, P. et al. The systematics of the Mongolepidida (Chondrichthyes) and the Ordovician origins of the clade. *PeerJ* **4**, e1850 (2016).
14. Vorobjeva, E. I. & Janvier, P. Observations to the note by E Vorobjeva: 'First discovery of Palaeozoic fishes on the territory of the Mongolian Republic'. *Geobios* **17**, 379–380 (1984).
15. Gegenbaur, C. *Grundriss der vergleichenden Anatomie* (Wilhelm Engelmann, 1874).
16. Alekseeva, R. E., Mendbayar, B. & Erlanger, O. A. *Brachiopods and Biostratigraphy of the Lower Devonian of Mongolia* (Nauka, 1981).
17. Alekseeva, R. E. *Devonian Biostratigraphy of Mongolia* (Nauka, 1993).
18. Mark-Kurik, E. in *Morphology, Phylogeny and Paleobiogeography of Fossil Fishes* (eds Elliott, D. K. et al.) 101–106 (Verlag Dr. Friedrich Pfeil, 2010).
19. Ørvig, T. Description, with special reference to the dermal skeleton, of a new radotinid arthrodire from the Gedinnian of Arctic Canada. *Colloq. Int. Cent. Natl Rech. Sci.* **218**, 43–71 (1975).
20. Olive, S., Goujet, D., Lelièvre, H. & Janjou, D. A new Placoderm fish (Acanthothoraci) from the Early Devonian Jauf Formation (Saudi Arabia). *Geodiversitas* **33**, 393–409 (2011).
21. Wängsjö, G. The Downtonian and Devonian vertebrates of Spitsbergen. IX. *Norsk Polarinstitutt Skrifter* **97**, 1–611 (1952).
22. Charest, F., Johanson, Z. & Cloutier, R. Loss in the making: absence of pelvic fins and presence of paedomorphic pelvic girdles in a Late Devonian antiarch placoderm (jawed stem-gnathostome). *Biol. Lett.* **14**, 20180199 (2018).
23. Dupret, V., Sanchez, S., Goujet, D. & Ahlberg, P. E. The internal cranial anatomy of *Romundina stellina* Ørvig, 1975 (Vertebrata, Placodermi, Acanthothoraci) and the origin of jawed vertebrates—anatomical atlas of a primitive gnathostome. *PLoS ONE* **12**, e0171241 (2017).
24. Stensiö, E. A. La cavité labyrinthique, l'ossification sclérotique et l'orbite de *Jagorina. Colloq. Int. Cent. Natl Rech. Sci.* **21**, 9–43 (1950).
25. Stensiö, E. A. Anatomical studies on the arthrodiran head. *K. Sven. Vetenskapsakad. Handl.* **9**, 1–419 (1963).
26. Goujet, D. *Les Poissons Placodermes du Spitsberg* (Cahiers de Paléontologie, Editions du CNRS, 1984).
27. Davis, S. P., Finarelli, J. A. & Coates, M. I. *Acanthodes* and shark-like conditions in the last common ancestor of modern gnathostomes. *Nature* **486**, 247–250 (2012).
28. Castiello, M. & Brazeau, M. D. Neurocranial anatomy of the petalichthyid placoderm *Shearsbyaspis oepiki* Young revealed by X-ray computed microtomography. *Palaeontology* **61**, 369–389 (2018).
29. Rosa, B. B., Melo, G. A. R. & Barbeitos, M. S. Homoplasy-based partitioning outperforms alternatives in Bayesian analysis of discrete morphological data. *Syst. Biol.* **54**, 373 (2019).
30. Brazeau, M. D. & Friedman, M. The characters of Palaeozoic jawed vertebrates. *Zool. J. Linn. Soc.* **170**, 779–821 (2014).
31. Zhu, M. et al. A Silurian placoderm with osteichthyan-like marginal jaw bones. *Nature* **502**, 188–193 (2013).
32. Giles, S., Friedman, M. & Brazeau, M. D. Osteichthyan-like cranial conditions in an Early Devonian stem gnathostome. *Nature* **520**, 82–85 (2015).
33. Miles, R. S. in *Interrelationships of Fishes* (eds Greenwood, P. H. et al.) 63–103 (Academic, 1973).
34. Zhu, M. Bone gain and loss: insights from genomes and fossils. *Natl Sci. Rev.* **1**, 490–492 (2014).
35. Janvier, P. *Les Céphalaspides du Spitsberg* (Éditions du CNRS, 1985).
36. Ørvig, T. Histologic studies of placoderms and fossil elasmobranchs. *Arkiv för Zoologi* **2**, 321–454 (1951).
37. Young, G. C. New information on the structure and relationships of *Buchanosteus* (Placodermi: Euarthrodira) from the Early Devonian of New South Wales. *Zool. J. Linn. Soc.* **66**, 309–352 (1979).
38. Miles, R. S. & Young, G. C. in *Problems in Vertebrate Evolution* (eds Andrews, S. M. et al.) 123–198 (Academic, 1977).
39. Stensiö, E. A. On the head of the macropetalichthyids. *Field Mus. Nat. Hist. Publ. Geol. Ser.* **4**, 87–197 (1925).
40. Ørvig, T. Notes on some paleozoic lower vertebrates from Spitsbergen and North America. *Nor. Geol. Tidsskr.* **37**, 285–353 (1957).
41. Sansom, R. Phylogeny, classification and character polarity of the Osteostraci (Vertebrata). *J. Syst. Palaeontol.* **7**, 95–115 (2009).
42. Schaeffer, B. The braincase of the holostean fish *Macrepistius*, with comments on neurocranial ossification in the Actinopterygii. American Museum Novitates 2459, 1–34 (1971).
43. Watson, D. M. S. The acanthodian fishes. *Phil. Trans. R. Soc. Lond. B* **228**, 49–146 (1937).
44. Burrow, C. J., Davidson, R. G., Blaauwen, den, J. L. & Newman, M. J. Revision of *Climatius reticulatus* Agassiz, 1844 (Acanthodii, Climatiidae), from the Lower Devonian of Scotland, based on new histological and morphological data. *J. Vertebr. Paleontol.* **35**, e913421 (2015).
45. Dean, M. N., Socha, J. J., Hall, B. K. & Summers, A. P. Canaliculi in the tessellated skeleton of cartilaginous fishes. *J. Appl. Ichthyol.* **26**, 263–267 (2010).
46. Atake, O. J., Cooper, D. M. L. & Eames, B. F. Bone-like features in skate suggest a novel elasmobranch synapomorphy and deep homology of trabecular mineralization patterns. *Acta Biomater.* **84**, 424–436 (2019).
47. Pearson, D. M. & Westoll, T. S. The Devonian actinopterygian *Cheirolepis* Agassiz. *Earth Environ. Sci. Trans. R. Soc. Edinb.* **70**, 337–399 (1979).
48. Giles, S. et al. Endoskeletal structure in *Cheirolepis* (Osteichthyes, Actinopterygii), an early ray-finned fish. *Palaeontology* **58**, 849–870 (2015).
49. Cloutier, R. in *Devonian Fishes and Plants* (eds Schultze, H.-P. & Cloutier, R.) 227–247 (Verlag Dr. Friedrich Pfeil, 1996).
50. Grande, L. & Bemis, W. E. Osteology and phylogenetic relationships of fossil and recent paddlefishes (Polyodontidae) with comments on the interrelationships of Acipenseriformes. *J. Vertebr. Paleontol.* Suppl. **11** (Suppl. 1), 1–121 (1991).
51. Eames, B. F. et al. Skeletogenesis in the swell shark *Cephaloscyllium ventriosum. J. Anat.* **210**, 542–554 (2007).
52. Venkatesh, B. et al. Elephant shark genome provides unique insights into gnathostome evolution. *Nature* **505**, 174–179 (2014).
53. Ryll, B., Sanchez, S., Haitina, T., Tafforeau, P. & Ahlberg, P. E. The genome of *Callorhinchus* and the fossil record: a new perspective on SCPP gene evolution in gnathostomes. *Evol. Dev.* **16**, 123–124 (2014).
54. Marconi, A., Hancock-Ronemus, A. & Gillis, J. A. Adult chondrogenesis and spontaneous cartilage repair in the skate, *Leucoraja erinacea. eLife Sci.* **9**, 2813 (2020).
55. King, B., Qiao, T., Lee, M. S. Y., Zhu, M. & Long, J. A. Bayesian morphological clock methods resurrect placoderm monophyly and reveal rapid early evolution in jawed vertebrates. *Syst. Biol.* **66**, 499–516 (2016).
56. Clement, A. M. et al. Neurocranial anatomy of an enigmatic Early Devonian fish sheds light on early osteichthyan evolution. *eLife Sci.* **7**, e34349 (2018).
57. Goloboff, P. A. & Catalano, S. A. TNT version 1.5, including a full implementation of phylogenetic morphometrics. *Cladistics* **32**, 221–238 (2016).
58. Ronquist, F. & Huelsenbeck, J. P. MrBayes 3: Bayesian phylogenetic inference under mixed models. *Bioinformatics* **19**, 1572–1574 (2003).
59. Lewis, P. O. A likelihood approach to estimating phylogeny from discrete morphological character data. *Syst. Biol.* **50**, 913–925 (2001).
60. Rambaut, A., Drummond, A. J., Xie, D., Baele, G. & Suchard, M. A. Posterior summarization in Bayesian phylogenetics using Tracer 1.7. *Syst. Biol.* **67**, 901–904 (2018).

61. *R: A Language and Environment for Statistical Computing* (R Foundation for Statistical Computing, 2019).
62. Maddison, W. P. and Maddison, D. R. Mesquite: a modular system for evolutionary analysis. Version 3.61 http://www.mesquiteproject.org (2019)
63. Louca, S. & Doebeli, M. Efficient comparative phylogenetics on large trees. *Bioinformatics* **34**, 1053–1055 (2017).
64. Swofford, D. L. *PAUP*. Phylogenetic Analysis Using Parsimony (*and Other Methods)* Version 4.0a166 (Sinauer Associates, 2003).

Acknowledgements

Author contributions

M.D.B. conceived and designed the study. M.D.B., A.J., Y.A. and E.Z. participated in all field seasons. R.P.D. and A.J. undertook preliminary computed tomography scanning and segmentation that revealed the fossil was a 'placoderm' and had endochondral bone. R.S. discovered the first vertebrate remains in the first field season at Yamaat Gol in 2010. S.G. undertook the segmentation of *Minjinia* with input from M.D.B. A.J. performed segmentation of *Diplacanthus* tissue. M.C. provided input on occipital comparative morphology of 'placoderms'. R.P.D. provided data and comparative analyses and data for endoskeletal tissue. Y.A. provided background on the geology, palaeontology and stratigraphy of the type location; E.Z. and Y.A. organized field logistics and permitting. M.D.B., S.G., M.C., R.P.D. and A.J. undertook the anatomical interpretation and prepared the figures. M.D.B. and S.G. conducted the phylogenetic analyses. R.S. conducted the parsimony branch support analyses. T.G. wrote the script for generating MrBayes partitions from TNT's character fits table and conducted the likelihood and model-fitting analyses. The manuscript was written by M.D.B., R.P.D. and S.G.

Competing interests

The authors declare no competing interests.

Additional information

Extended data is available for this paper at https://doi.org/10.1038/s41559-020-01290-2.

Supplementary information is available for this paper at https://doi.org/10.1038/s41559-020-01290-2.
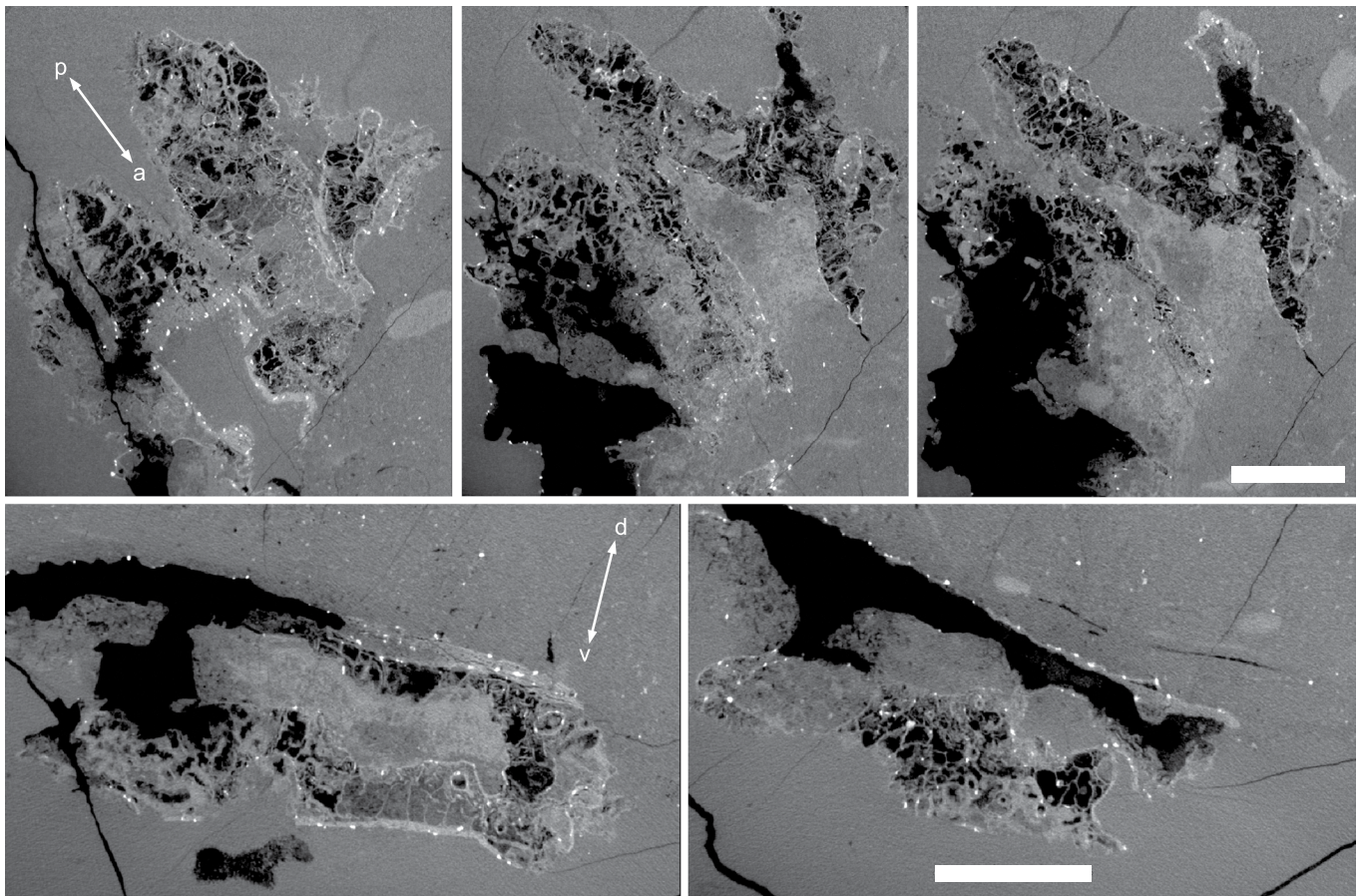
Correspondence and requests for materials should be addressed to M.D.B.

Peer review information Peer reviewer reports are available.
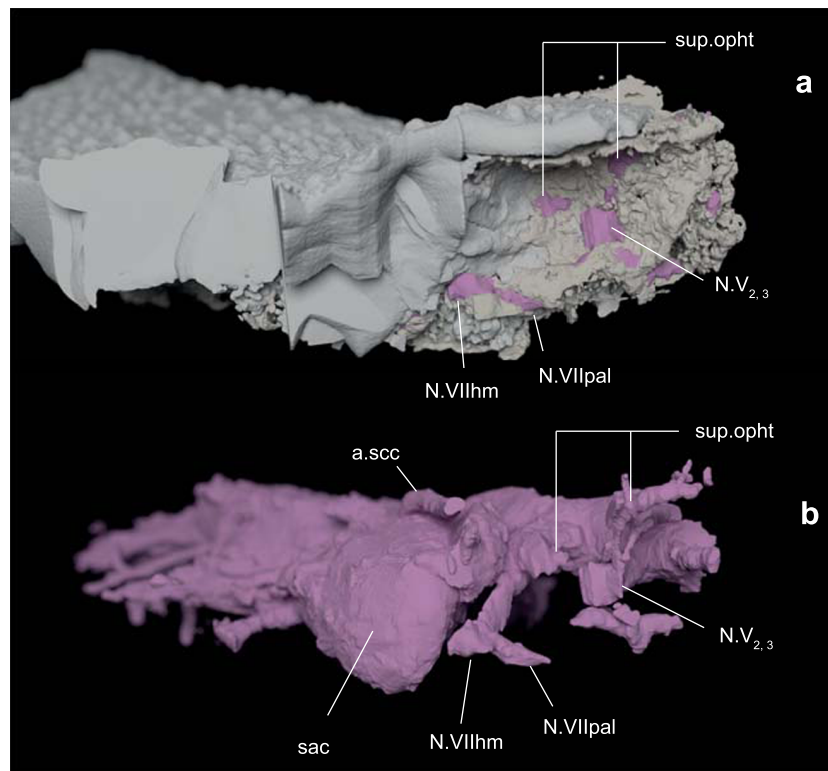
Reprints and permissions information is available at www.nature.com/reprints.

Publisher's note Springer Nature remains neutral with regard to jurisdictional claims in published maps and institutional affiliations.
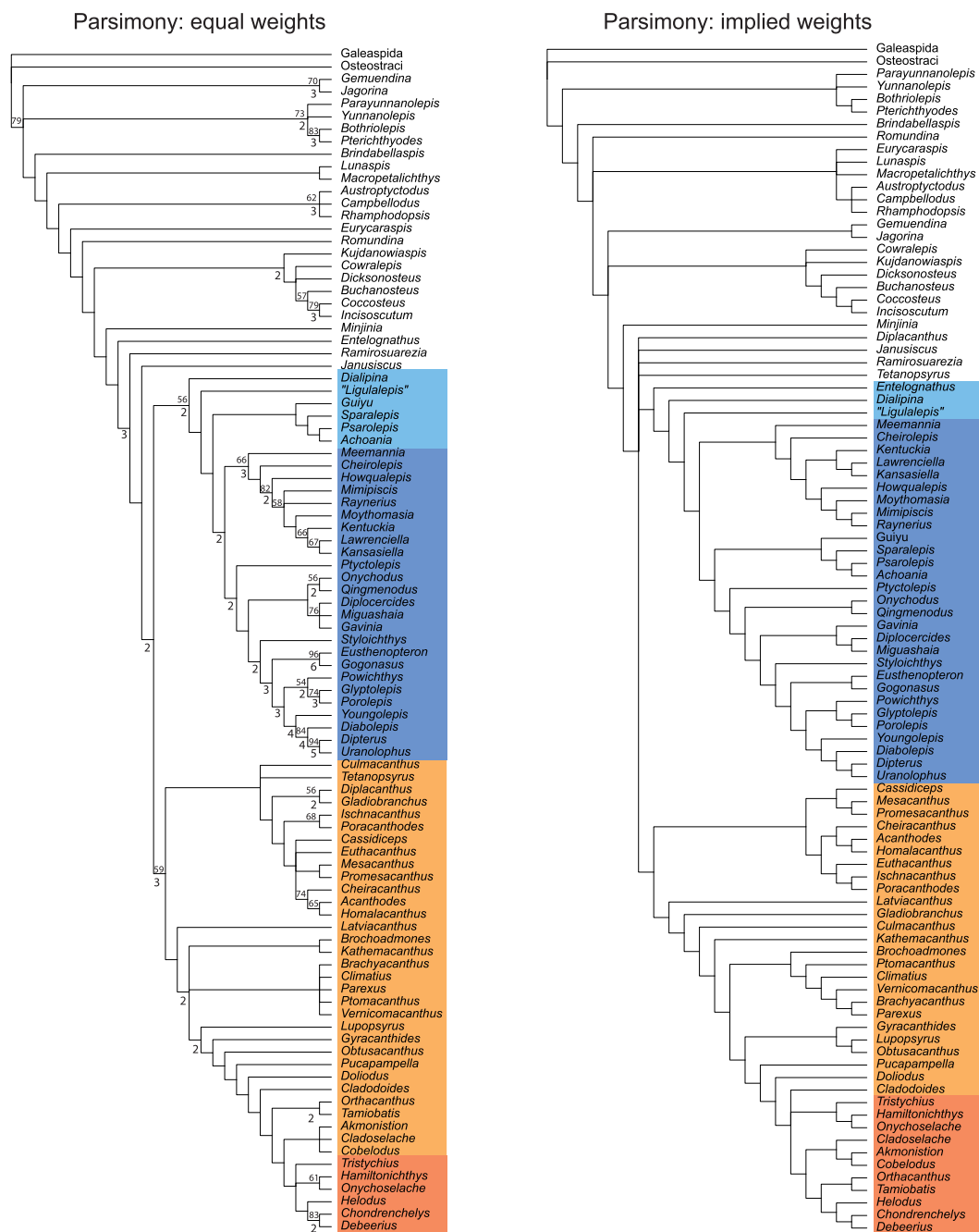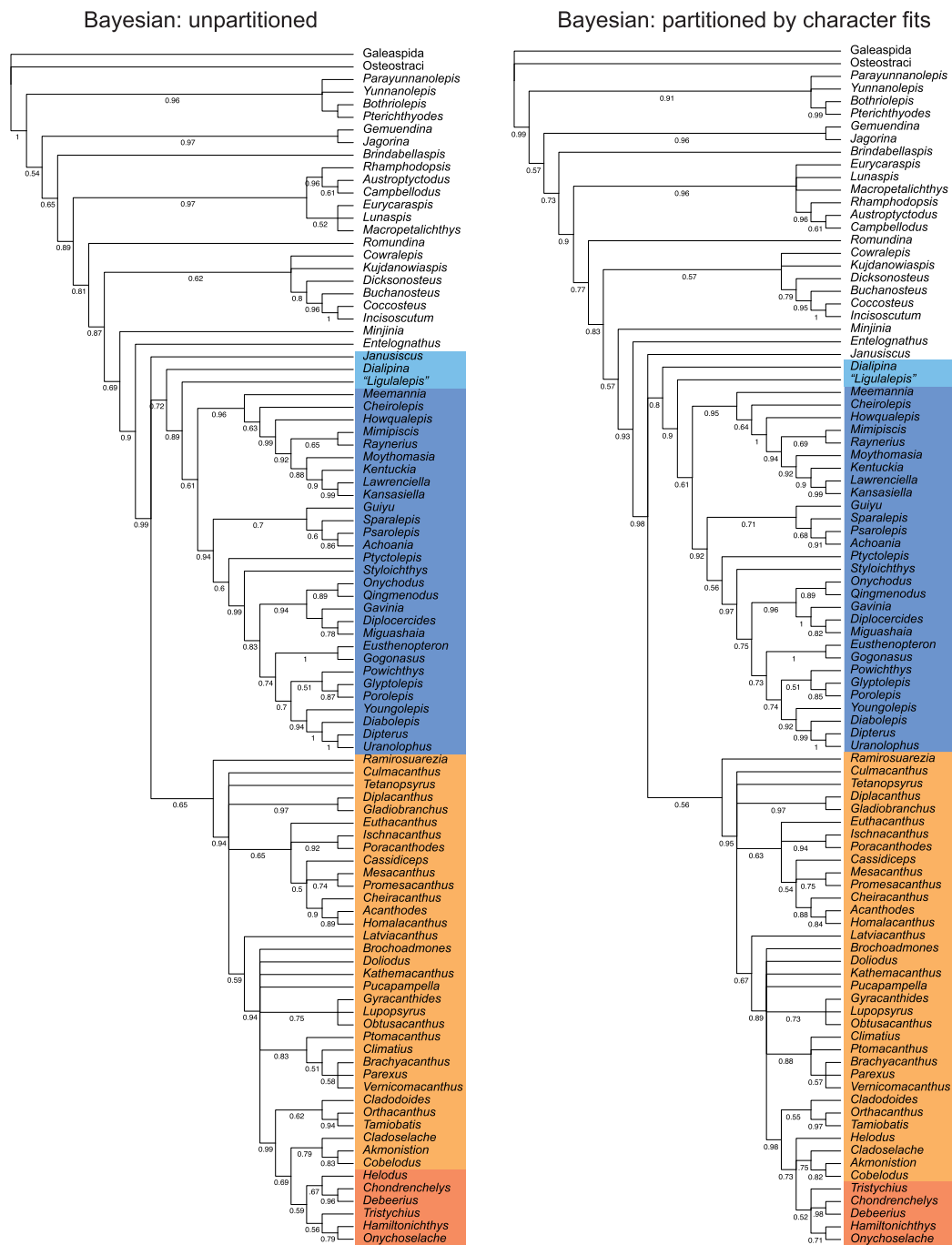
Extended Data Fig. 1 | Tomograms of endoskeletal ossification in MPC-FH100/9.1, *Minjinia turgenensis*. Top row: semi-coronal sections through braincase. Double-headed arrows indicate anterior-posterior (a-p) dorsal-ventral (d-v) axes. Bottom row: semi-transverse sections through posterior part of endocranium. Voids of black space represent mouldic preservation. Scale bars, 10 mm and apply across each row of panels.
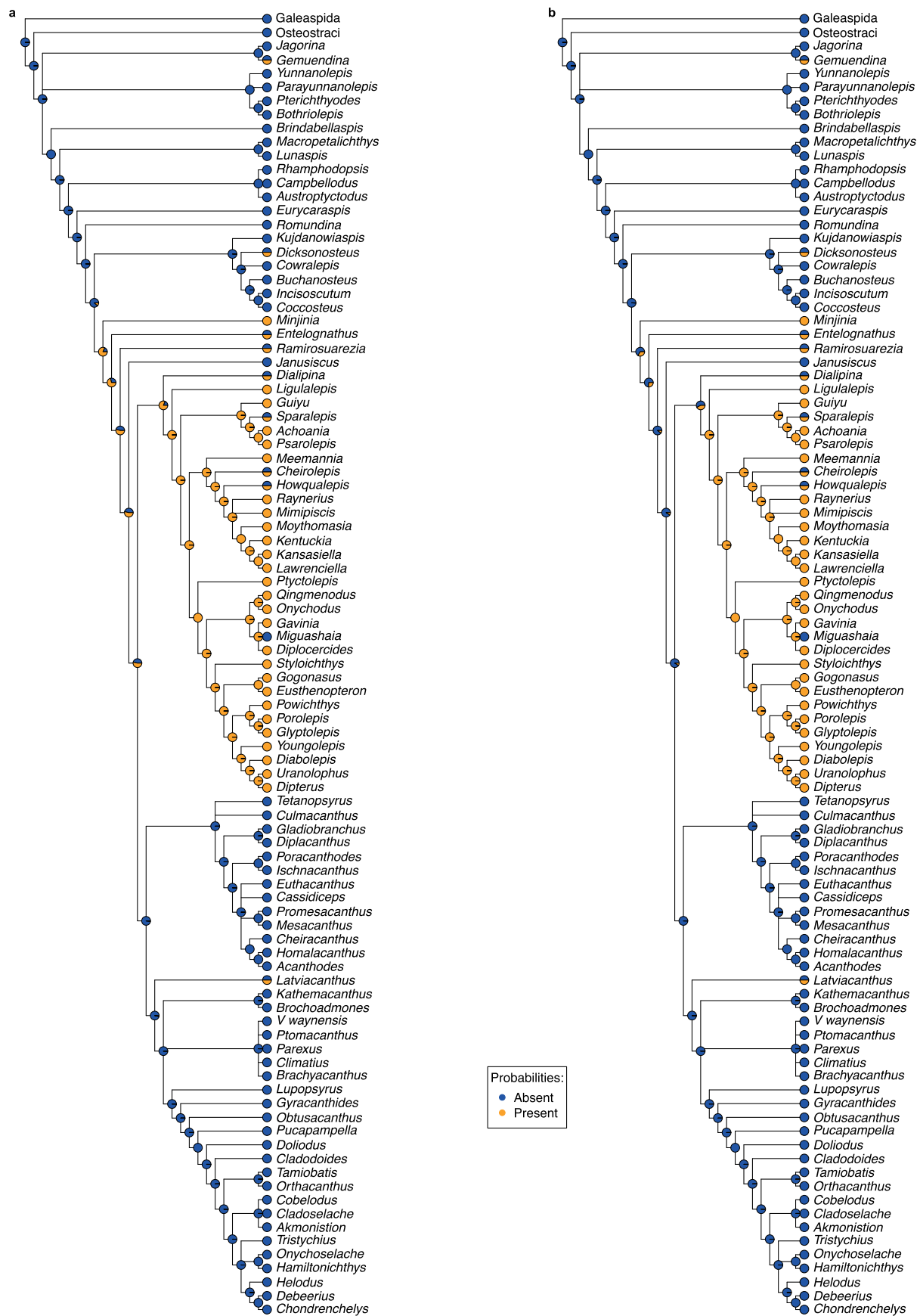
Extended Data Fig. 2 | Right orbital wall and innervation pattern of MPC-FH100/9.1, *Minjinia turgenensis*. a, Orbit in anterolateral view showing position of nerve openings (pink infill). **b**, Endocast in the same perspective showing the relationship between nerve canals and endocast. a.scc, anterior semicircular canal; N.V$_{2,3}$ trunk of the trigeminal nerve canal for branches 2 and 3; N.VIIhm, hyomandibular branch of facial nerve canal; N.VIIpal, palatine branch of facial nerve canal; sac, sacculus; sup.opht, canal for supra-ophthalmic nerve.
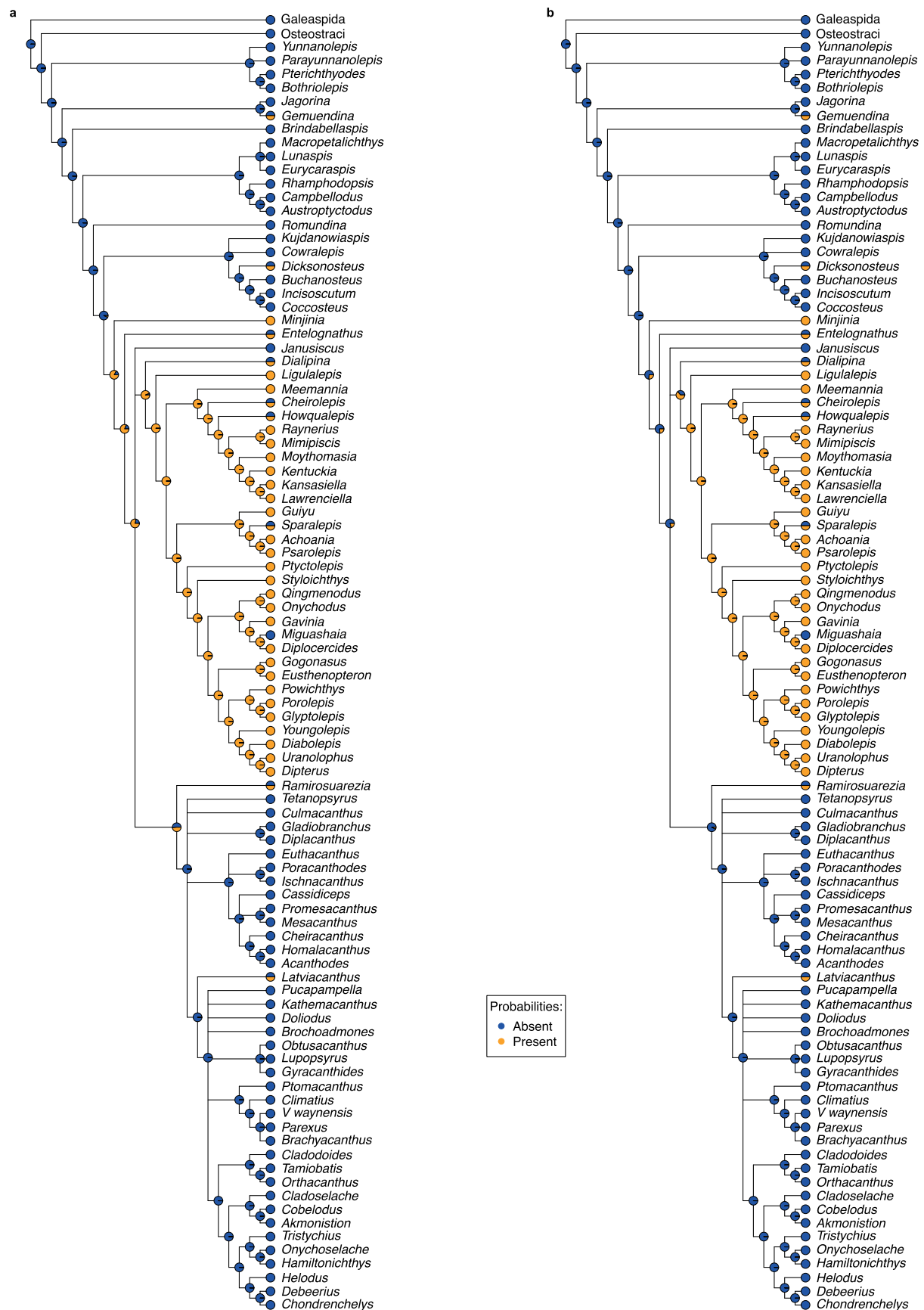
Parsimony: equal weights

Parsimony: implied weights

Extended Data Fig. 3 | Results of phylogenetic parsimony analysis. Dataset consists of 95 taxa and 284 characters. Both trees are strict consensus topologies. Equal weights parsimony analysis using the ratchet resulted in 240 trees with a length of 831 steps. Implied weights parsimony analysis using random addition sequence + branch-swapping resulted in 8 optimal trees with score 85.20513. Double-digit figures above internal branches are bootstrap values of 50% and over; single-digit figures below branches are Bremer decay index values. Blue shading: osteichthyan total group (dark blue: crown group); orange shading: chondrichthyan total group (dark orange: crown group).

Extended Data Fig. 4 | Results of Bayesian phylogenetic analysis using both partitioned and unpartitioned data. Majority-rules consensus trees with posterior probabilities shown along branches. Blue shading: osteichthyan total group (dark blue: crown group); orange shading: chondrichthyan total group (dark orange: crown group).

Extended Data Fig. 5 | Likelihood ancestral state mapping of endochondral bone on equal weights parsimony results. a, ARD, all rates different model; **b**, ER, equal rates model.

Extended Data Fig. 6 | Likelihood ancestral state mapping of endochondral bone on unpartitioned Bayesian analysis results. a, ARD, all rates different model; **b**, ER, equal rates model.

nature research

Corresponding author(s): Martin D Brazeau

Last updated by author(s): Jul 22, 2020

Reporting Summary

Nature Research wishes to improve the reproducibility of the work that we publish. This form provides structure for consistency and transparency in reporting. For further information on Nature Research policies, see our Editorial Policies and the Editorial Policy Checklist.

Statistics

For all statistical analyses, confirm that the following items are present in the figure legend, table legend, main text, or Methods section.

n/a	Confirmed	
☒	☐	The exact sample size (*n*) for each experimental group/condition, given as a discrete number and unit of measurement
☒	☐	A statement on whether measurements were taken from distinct samples or whether the same sample was measured repeatedly
☒	☐	The statistical test(s) used AND whether they are one- or two-sided *Only common tests should be described solely by name; describe more complex techniques in the Methods section.*
☒	☐	A description of all covariates tested
☒	☐	A description of any assumptions or corrections, such as tests of normality and adjustment for multiple comparisons
☒	☐	A full description of the statistical parameters including central tendency (e.g. means) or other basic estimates (e.g. regression coefficient) AND variation (e.g. standard deviation) or associated estimates of uncertainty (e.g. confidence intervals)
☒	☐	For null hypothesis testing, the test statistic (e.g. *F*, *t*, *r*) with confidence intervals, effect sizes, degrees of freedom and *P* value noted *Give P values as exact values whenever suitable.*
☐	☒	For Bayesian analysis, information on the choice of priors and Markov chain Monte Carlo settings
☒	☐	For hierarchical and complex designs, identification of the appropriate level for tests and full reporting of outcomes
☒	☐	Estimates of effect sizes (e.g. Cohen's *d*, Pearson's *r*), indicating how they were calculated

Our web collection on statistics for biologists contains articles on many of the points above.

Software and code

Policy information about availability of computer code

Data collection	*Provide a description of all commercial, open source and custom code used to collect the data in this study, specifying the version used OR state that no software was used.*
Data analysis	Mimics 19.0 (www.materialisesoftware.com); PAUP v4.0b166; TNT v1.5; MrBayesv 3.27; Tracer 1.7; R v3.6.1, Mesquite 3.61

For manuscripts utilizing custom algorithms or software that are central to the research but not yet described in published literature, software must be made available to editors and reviewers. We strongly encourage code deposition in a community repository (e.g. GitHub). See the Nature Research guidelines for submitting code & software for further information.

Data

Policy information about availability of data

All manuscripts must include a data availability statement. This statement should provide the following information, where applicable:

- Accession codes, unique identifiers, or web links for publicly available datasets
- A list of figures that have associated raw data
- A description of any restrictions on data availability

The holotype specimen of Minjinia turgenensis will be permanently deposited in the collections of the Institute of Paleontology, Mongolian Academy of Science. Original tomograms are available at (doi:10.6084/m9.figshare.12301229) and rendered models are available at (doi:10.6084/m9.figshare.12301223). The phylogenetic character list and dataset are available as Supplementary Information S1 and S2. The LifeScience Identifier for Minjinia turgenensis is urn:lsid:zoobank.org:act:82A1CEEC-B990-47FF-927A-D2F0B59AEA87

Field-specific reporting

Please select the one below that is the best fit for your research. If you are not sure, read the appropriate sections before making your selection.

☐ Life sciences ☐ Behavioural & social sciences ☒ Ecological, evolutionary & environmental sciences

For a reference copy of the document with all sections, see nature.com/documents/nr-reporting-summary-flat.pdf

Ecological, evolutionary & environmental sciences study design

All studies must disclose on these points even when the disclosure is negative.

Study description	We describe the braincase, brain endocavity, and skeletal tissue of a 410 million-year-old fossil fish braincase from western Mongolia. The braincase data reveal the presence of endochondral bone
Research sample	One specimen of a braincase from the Early Devonian of Mongolia. This is the only known example.
Sampling strategy	Excavation of a fossil fish-bearing layer in the Early Devonian rocks of western Mongolia.
Data collection	The specimen was collected in the field. It was subjected to three rounds of computed tomography scanning following successive removal of surrounding matrix.
Timing and spatial scale	The specimen was collected in the summer of 2012.
Data exclusions	NA
Reproducibility	The specimen will be permanently housed in the collections of the Institute of Palaeontology, Mongolian Academy of Science and will be available for study. The computed tomography data will be archived permanently online along with the surface models.
Randomization	NA
Blinding	NA

Did the study involve field work? ☒ Yes ☐ No

Field work, collection and transport

Field conditions	Dry summer conditions.
Location	Turgen Strictly Protected Area, Uvs aimag, Mongolia
Access & import/export	The material was collected under an agreement between the lead author's then host institution (Naturalis Biodiversity Centre) and the Paleontological Centre of the Mongolian Academy of Science (now Institute of Paleontology, Mongolian Academy of Science). Through this agreement, we obtained all necessary permissions for fieldwork in Mongolia and excavation work in strictly protected areas. The work was conducted under supervision of the superintendent at the Turgen Strictly Protected Area.
Disturbance	The fossils came from a restricted bed in a hillside and were excavated with hand tools causing a scar in the hillside. The excavations were small (ca. 1-4 cubic meters) and the resulting excavations were back-filled with talus and the natural contours restored.

Reporting for specific materials, systems and methods

We require information from authors about some types of materials, experimental systems and methods used in many studies. Here, indicate whether each material, system or method listed is relevant to your study. If you are not sure if a list item applies to your research, read the appropriate section before selecting a response.

Materials & experimental systems

n/a	Involved in the study
☒ ☐	Antibodies
☒ ☐	Eukaryotic cell lines
☐ ☒	Palaeontology and archaeology
☒ ☐	Animals and other organisms
☒ ☐	Human research participants
☒ ☐	Clinical data
☒ ☐	Dual use research of concern

Methods

n/a	Involved in the study
☒ ☐	ChIP-seq
☒ ☐	Flow cytometry
☒ ☐	MRI-based neuroimaging

Palaeontology and Archaeology

Specimen provenance	The specimens come from the Turgen Strictly Protected area in the Uvs aimag of western Mongolia. Paleontological permits were secured from the Ministry of Culture, Education and Science (20 June, 2012; Reg. no.7, signed for by U Sukhbaatar).
Specimen deposition	Specimens are deposited in the Natural History Museum, Ulaanbaatar
Dating methods	NA

☐ Tick this box to confirm that the raw and calibrated dates are available in the paper or in Supplementary Information.

Ethics oversight	No ethical approval or guidance was required.

Note that full information on the approval of the study protocol must also be provided in the manuscript.